Influence of deformed-nucleus level densities on statistical model calculations for high-spin fission

S. E. Vigdor and H. J. Karwowski*
Indiana University Cyclotron Facility, Bloomington, Indiana 47405
(Received 19 March 1982)

Inappropriate formulations for nuclear level densities, based in part on an assumption of spherical symmetry, have often been employed in statistical model calculations of the competition between decay modes of nuclei at high spin and excitation. We investigate the influence on such calculations of nuclear deformation effects in the level densities, at both the saddle-point shapes relevant to fission and the most probable shapes reached in particle evaporation. The deformation effects are included in a Fermi-gas formalism in two stages, first assuming complete independence of rotational and intrinsic degrees of freedom, and subsequently allowing for a deformation-dependent cutoff with increasing temperature in the collective enhancement of the level densities. The latter effect gives rise, in the absence of shell and pairing corrections, to a progressive increase with increasing temperature in the most probable daughter-nucleus deformation for particle emission. The most significant effects of the deformed-nucleus level densities on calculated decay properties for $^{6}Li+^{197}Au\rightarrow^{203}Pb$, at several bombarding energies, are an increase in the cross section and a decrease in the anisotropy for fission fragments. Ambiguities in the details of the collective cutoff yield a sizable uncertainty in the quantitative extent of the fission enhancement. Relative measurements for different entrance channels to the same compound nucleus which may be sensitive to the collective cutoff are illustrated by calculations for $^{22}Ne+^{180}Hf$ vs $^{6}Li+^{197}Au$ fusion-fission.

NUCLEAR REACTIONS Fission-evaporation competition in decay of ^{203}Pb from high excitation and angular momentum. Statistical model calculations for deformed nuclei incorporate collective level density enhancements which fade with increasing temperature.

I. INTRODUCTION

In heavy-ion induced fusion and deeply inelastic reactions, nuclei are often produced at quite high angular momentum, excitation energy, and deformation. Investigations of the decay products, especially of fission fragments, from such highly excited nuclei are potentially useful in probing both the mechanism for the initial formation of the decaying nucleus[1] and its structure at high spin.[1-7] However, there are often serious ambiguities in the quantitative interpretation of decay measurements, for which one relies on some form of statistical model analysis[1-8] of the competition among the many decay channels open at high excitation. Such analyses assume that the relative widths for different decay modes are determined purely by considerations of potential barrier penetrabilities and accessible phase space (i.e., the number of relevant open channels). Even if one grants the appropriateness of this basic assumption, the detailed statistical model calculations of inverse reaction cross sections for particle emission, and of nuclear level densities relevant to both particle and fission decay, are plagued by considerable theoretical uncertainties and by a lack of opportunity to test these theories independently for nuclei with suitable properties. Thus, inverse reaction (i.e., fusion) cross sections for nucleons and α particles can be measured for target nuclei in their ground states, but there is no direct experimental guidance on how to extrapolate from such measurements to the "hot," and possibly highly deformed,

nuclei of interest.[2,8–10] Similarly, theoretical calculations of level densities have been compared with direct experimental results[1,11–15] only at relatively low excitation and spin, and over the limited range of deformations provided by nature for particle-stable or nearly stable nuclei.

The best chance for progress in understanding the decay competition in hot, high-spin nuclei lies in identifying theoretically expected changes in level densities and penetrabilities with increasing spin, excitation, and deformation, and in incorporating such changes in analyses of systematic measurements of many decay properties. The encouraging results of such a comprehensive program of experiments and statistical model analyses of fusion-product decay have been reported in the preceding paper.[16] In the present paper, we describe in detail our improvements to standard statistical model treatments of nuclear deformation effects on the excitation energy and spin dependence of level densities. In this work we have been guided by the theory of deformed-nucleus level densities developed by Ericson[17] and by Bjørnholm, Bohr, and Mottelson.[18]

It is crucial in any calculation of fission-evaporation competition to consider the difference in level densities between the strongly deformed saddle-point and more mildly deformed equilibrium shapes of the nucleus. This difference is very sensitive to the changes with deformation in the density of single-particle levels at the Fermi energy, and in the potential energy surface relative to which one must measure the energy available for intrinsic excitations. These two indirect effects of the deformation have been incorporated, via adjustable parameters, in previous statistical model analyses. However, the role of deformation in establishing an energy-favored spin orientation (in a body-fixed reference frame) has usually been neglected; i.e., the number of levels of a given excitation energy and total angular momentum has been deduced *under the implicit assumption of spherical symmetry* from the thermodynamically calculable density of states with a given spin *projection* along some chosen axis.[4–6,19] This approach is inappropriate for any body-fixed axis in a deformed nucleus and is expected[13,14,17,18] to lead to large errors in the *absolute* values of the level density for deformed nuclei at relatively low excitation. The error introduced with this approach in the *relative* level densities for fission versus particle emission from a highly excited nucleus is not clear from previous work, and is the subject of the present investigation.

In taking explicit account of the deformation in enumerating levels of given spin, one must decide whether to include collective (rotational) degrees of freedom independently of the intrinsic nuclear excitations,[8,17,18] and if so, whether to include them in a similar manner at the saddle-point and equilibrium shapes. In the present work, we investigate the influence of the collective excitations in two stages. First we include the full collective enhancement of level densities (corresponding to complete independence of the collective and intrinsic degrees of freedom) at all deformations and temperatures, yielding a treatment similar in spirit to that of Jensen and co-workers.[7] We then propose a new method for incorporating the expected dilution of the collective enhancement with increasing temperature, which must arise when the single-particle Coriolis excitations associated with the rotational motion become accessible.[18] In our approach the net effect of the collective enhancement "fadeout" is a progressive increase with temperature of the most probable deformation reached in particle emission processes. We include the effect of this increasing deformation on the transmission coefficients for particle decay[10,20,21] as well as on the level densities.

The general features and underlying assumptions of our statistical model calculations are discussed in Sec. II, along with the formulas used to evaluate the fission (σ_f) and particle-emission ($\sigma_{n,p,\alpha}$) cross sections and the fission fragment anisotropy (γ_f) once the level densities are known. In Sec. II, we also present our method for estimating transmission coefficients for deformed nuclei. A detailed description of the level density treatment in conventional codes,[4–6] and of the two stages of the deformed-nucleus treatment in our code, is given in Sec. III. Differences among the various treatments are illustrated by comparing calculations of the fission probability as a function of spin and chance (i.e., the stage during the evaporation chain at which fission occurs), and of σ_f, σ_α, and γ_f as a function of bombarding energy, for the system $^{6}\mathrm{Li}+^{197}\mathrm{Au}\rightarrow^{203}\mathrm{Pb}$. All of these calculations assume a nuclear potential energy surface and intrinsic level density parametrization consistent with the rotating-liquid-drop (RLDM) (Ref. 22) and noninteracting Fermi gas (NIFG) (Refs. 8, 11, and 23) models of the nucleus; we thereby exclude from our present considerations the additional complicating influence of the variation in shell and pairing structure corrections with spin, deformation, and excitation.[2,3,24,25] The comparison of our statistical model calculations with experimental results in the preceding paper suggests that this neglect of microscopic corrections is appropriate at the high tem-

peratures which apparently dominate the observed decay.[16] The conclusions of the present work are summarized in Sec. IV.

II. THE STATISTICAL MODEL CODE

A. General features and assumptions

Our calculations have been carried out with an extensively modified version of the code MB-II (Ref. 26), the logistics of which have been described in detail elsewhere[2,4,10]; we call the new version MBEGAT. As is conventional in statistical model analyses, we assume (for the purposes of the present paper, but see Ref. 16) that the decaying nucleus has reached thermal equilibrium, so that the mechanism of its formation is reflected at most in the excitation energy and spin distributions of the populated states, and not at all in their structure. The relative probabilities for different decay modes are then determined by barrier penetrabilities and accessible phase space.

The relevant level densities are evaluated *as if* a given decay process always led to a given well-defined nuclear shape, corresponding in principle to the most probable deformation (at the appropriate excitation and spin) in the final nucleus reached via particle emission, or to the phase-space "bottleneck" along the most probable path to fission (the "transition state" of Bohr and Wheeler[27]). In keeping with standard terminology, we will refer to these deformations henceforth as "yrast" (or "equilibrium") and "saddle-point" shapes, respectively; however, it must be understood that they are not necessarily simply related to features of the *actual* potential energy surface (PES) of the *"cold"* nucleus. Indeed, with increasing nuclear temperature one expects[24,25] shell and pairing corrections to the PES and to level densities to counterbalance one another progressively more completely, so that the relevant deformation probabilities (at least those derived from the density of *intrinsic* excitations) evolve toward the values characteristic of a RLDM-NIFG nucleus. In addition, we will argue in Sec. III C that, even at temperatures where shell and pairing effects are already negligible, allowance for the "fadeout" of the collective enhancement to level densities may lead to a further temperature dependence of the effective "yrast" deformation.

The relative decay widths for fission (Γ_f) and for particle emission (Γ_ν, $\nu=n,p,\alpha$) from a nucleus of spin I and excitation energy E^* are evaluated in the code as follows:

$$\Gamma_f(E^*,I) \propto \int_0^{[E^*-E_{\rm sad}(I)]} \rho_f[E^*-E_k,I]dE_k \ ; \tag{1}$$

$$\Gamma_\nu(E^*,I) \propto (2s_\nu+1)\sum_{l=0}^{\infty}\sum_{J=|I-l|}^{I+l}\int_0^{[E^*-E_{\rm yr}(J)-B_\nu]} \rho_\nu[E^*-B_\nu-\epsilon,J]T_\nu^l(\epsilon)d\epsilon \ . \tag{2}$$

Here the potential energies corresponding to the effective saddle-point and yrast shapes, as defined above, are given by $E_{\rm sad}(I)$ and $E_{\rm yr}(J)$, where J is the angular momentum of the daughter nucleus reached by particle emission; the corresponding level densities ρ_f and ρ_ν are calculated as functions of excitation energy and total angular momentum according to one of the three prescriptions described in Sec. III; s_ν and B_ν are, respectively, the intrinsic spin and the s-wave separation energy of the emitted particle; E_k is the kinetic energy associated with the fission distortion; ϵ, l, and $T_\nu^l(\epsilon)$ are the c.m. kinetic energy, the orbital angular momentum, and the associated transmission coefficient of the emitted particle with respect to the daughter nucleus. In writing Eq. (1) we have implicitly assumed that the *fission* barrier transmission is unity above and zero below the barrier height. This classical approximation, introduced for convenience, is well justified in the present calculations, where the fission decay is overwhelmingly dominated by processes occurring well above the barrier.

The partial widths Γ_f and Γ_ν are calculated for all relevant values of E^* and I (in 1 MeV by $1\hbar$ bins), for each nuclide in the chain deexciting the compound nucleus (CN). The CN itself starts with a unique excitation energy and a spin distribution $\sigma_{\rm CN}(I)$ specified as input to the calculation. Evaluation of the evaporation widths as a function of ϵ and J then yields the population profiles $\sigma_{N,Z}(E^*,I)$ for each subsequent nuclide (N,Z) in the decay chain. The fraction of $\sigma_{N,Z}(E^*,I)$ which goes in turn into one of the four (f,n,p,α) decay modes is given by the ratio of the corresponding partial width to the sum of all four partial widths. In the present calculations we assume that γ decay

does not compete effectively with the above modes, but rather occurs only at the end of the chain when fission and particle emission become energetically inaccessible. To save computing time, we further neglect here the very small contributions[16] from decay processes involving multiple charged-particle evaporation or fission after charged-particle evaporation.

The decay widths calculated for a given level density treatment and, to a lesser extent, the relative values for different level density formulations, are sensitive to the values chosen for the input parameters which determine such quantities as $E_{\rm sad}(I)$, $E_{\rm yr}(J)$, B_ν, $T_\nu^I(\epsilon)$, and $\sigma_{\rm CN}(I)$. With a few exceptions which are noted explicitly in subsequent sections, these and other input data are chosen via the prescriptions explained in detail in Sec. IV B of the preceding paper.[16]

B. Fission-fragment angular distribution

It is useful to consider the angular distribution $W_f(\theta)$ of the fission fragments as well as the total cross section σ_f because the two quantities exhibit complementary sensitivities to the nuclear structure parameters which influence the fission decay widths.[16,28] The evaluation of $W_f(\theta)$ in MBEGAT follows essentially the geometrical model proposed by Halpern and Strutinski[29] (see also Ref. 30). Assuming that the fragments separate along the saddle-point symmetry axis, a fissioning nucleus of total angular momentum I, projection K along the symmetry axis, and zero projection along the beam direction ($M=0$), will be characterized by an angular distribution

$$W_{I,K}(\theta) \propto [\sin^2\theta - K^2/I^2]^{-1/2} , \quad \text{for } \sin^2\theta > \frac{K^2}{I^2} . \tag{3}$$

In the limit $K=0$, Eq. (3) reduces to the more familiar form

$$W_{K=0}(\theta) \propto 1/\sin\theta . \tag{4}$$

The $M=0$ assumption is strictly valid only if the CN is formed from spinless projectile and target nuclei, and even then, only for first-chance fission, since neutron emission may change M. If $M \ll I$, however, as is the case for the dominant contributions to our calculated fission yields, the $M=0$ approximation introduces only very small errors ($\lesssim$ a few percent) in $W_f(\theta)$,[30] and is sufficient for our purposes.

For fission of a hot nucleus (nuclear temperature τ) of spin I, the angular distribution is obtained by summing Eq. (3) over the full expected distribution of K values:

$$W_{I,\tau}(\theta) = \sum_{K=0}^{I} W_{I,K}(\theta)\eta_{I,\tau}(K) \rightarrow \int_{K=0}^{(I+1/2)} W_{I,K}(\theta)\eta_{I,\tau}(K)dK , \tag{5}$$

where we have denoted the probability of finding the fissioning nucleus with projection K by $\eta_{I,\tau}(K)$, and we have made the usual classical (high-spin) replacement of the summation by an integral. We make the standard assumption[29,30] that the K distribution is "frozen" at the saddle point, and for computational convenience we use the Gaussian form

$$\eta_{I,\tau}(K) \propto \exp(-K^2/2K_{0_{\rm sad}}{}^2), \quad 0 \le K \le I , \tag{6}$$

where

$$K_{0_{\rm sad}}{}^2 \equiv (\mathcal{I}_{\rm eff})_{\rm sad}\tau/\hbar^2 \equiv (\mathcal{I}_\perp)_{\rm sad}(\mathcal{I}_{||})_{\rm sad}\tau/\hbar^2[(\mathcal{I}_\perp)_{\rm sad} - (\mathcal{I}_{||})_{\rm sad}] ; \tag{7}$$

$\mathcal{I}_{||}$ and $\mathcal{I}_\perp$ are the moments of inertia (for rotations about the symmetry axis and about an orthogonal axis, respectively) evaluated at the saddle-point deformation for spin I. As will be seen in Sec. III B, the Gaussian approximation to the K dependence of the saddle-point state density is valid in the limit

$$E^* \gg E_{\rm sad}(I) + \hbar^2K^2/2(\mathcal{I}_{\rm eff})_{\rm sad} ;$$

our failure to include in $\eta_{I,\tau}(K)$ the appreciable deviations from a Gaussian expected in the tail of the K distribution (for $K \gtrsim 2K_0$) introduces a small error in $W_f(\theta)$ which nearly cancels that arising from the $M=0$ assumption.

Combining Eqs. (3), (5), and (6) we obtain the following analytical expression for the angular distribution at given spin and temperature:

$$W_{I,\tau}(\theta)=C(I,\tau)\exp[-(I+\tfrac{1}{2})^2\sin^2\theta/4K_{0_{\rm sad}}{}^2]J_0[i(I+\tfrac{1}{2})^2\sin^2\theta/4K_{0_{\rm sad}}{}^2]\ , \tag{8}$$

where J_0 is a zero-order Bessel function of imaginary argument. In the code, Eq. (8) is applied to fission from a given spin in a given nuclide in the decay chain (i.e., a given "chance" of fission). For fission following particle emission, the effective saddle-point temperature τ, and hence $K_0{}^2$, are determined from the calculated E^*-I population profiles, to correspond to the *mean* excitation energy contributing to fission from the appropriate spin and chance. The normalization factor $C(I,\tau)$ [which incorporates all angle-independent factors appearing elsewhere[30] in expressions analogous to Eq. (8)] is determined by requiring angular integration of Eq. (8) to reproduce the MBEGAT prediction for σ_f from that spin and chance. The final calculated angular distribution is obtained by summation over all spins in each fissioning nuclide, and over all fissioning nuclides:

$$W(\theta)=\sum_{\text{chance}}\sum_{I}W_{I,\tau}(\theta)\ . \tag{9}$$

For purposes of comparing different calculations, or calculations with measurements, the fission-fragment angular distributions are most easily characterized by the anisotropy

$$\gamma_f\equiv W_f(170°)/W_f(90°)\ , \tag{10}$$

which can be seen from Eq. (8) to be quite sensitive to the ratio I/K_0. Specifically, γ_f increases as I increases for roughly constant K_0, or as τ and K_0 decrease for fixed I. The overall anisotropy, corresponding to Eq. (9), is thus particularly sensitive to the distribution of the fission cross section with respect to spin and chance.[16,28]

C. Transmission coefficients for particle emission

For reasons explained in the preceding paper,[16] the present calculations are based on the standard assumption that the inverse reaction (namely, fusion on hot target nuclei) cross sections for particle emission are well approximated by *total reaction* cross sections for *cold* target nuclei. Thus we generate the transmission coefficients $T_\nu^l(\epsilon)$ appearing in Eq. (2) from optical model (OM) calculations, using potential parameters deduced in low-energy n, p, and α elastic scattering studies[31] for targets in the Pb region. Strictly, the OM calculations should solve the Schrödinger equation for scattering potentials which deviate from spherical symmetry, reflecting the effective yrast deformation in the daughter nuclei reached by particle decay.[10] In practice, however, the RLDM yrast deformations[22] for the mass and spin range of interest here are sufficiently small (major-to-minor axis ratios typically less than 1.10) that the effect of deformation on the $T_\nu^l(\epsilon)$ can be safely neglected. Thus, for most of the calculations reported in the present paper, we use standard shapes for the n, p, and α scattering potentials, e.g., real central nuclear wells of Woods-Saxon form:

$$U_N(r)=-V_0\{1+\exp[(r-R_0)/a_R]\}^{-1}\ . \tag{11}$$

The neglect of deformation effects on the $T_\nu^l(\epsilon)$ is no longer necessarily justified once we allow for the "fadeout" of the collective level density enhancement, since then the deformations most probably reached in particle decay may considerably exceed the RLDM values (see Sec. III C). In these cases we approximate the solution of the Schrödinger equation for deformed OM potentials by a method similar in spirit to, although differing in detailed execution from, those applied in Refs. 10, 20, and 21. We treat a range of deformed nuclei with axial and reflection symmetry, for which contours of constant matter density (or constant nuclear potential) are assumed to have the form

$$R(\theta)=R_0[\,1+\alpha_0+\alpha_2P_2(\cos\theta)+\alpha_4P_4(\cos\theta)]\ , \tag{12}$$

where θ is the angular deviation from the symmetry axis. (For a given value of the quadrupole deformation parameter α_2, α_4 is always chosen to minimize the total RLDM potential energy and α_0 to maintain the volume of the spherical nucleus; see the Appendix.)

The approximation method we use for the deformed-nucleus transmission coefficients is a compromise between the demands of computing speed and accuracy. We do not solve the full three-dimensional Schrödinger equation for a deformed, complex potential of realistic shape. Rather, we consider a series of one-dimensional radial equations, each involving an effective central potential appropriate to a (classical) particle incident at some well-defined angular orientation θ with respect to the symmetry axis of the target nucleus. This "equivalent spheres" approximation has been

applied in most previous work[10,20,21,32] as well, with varying degrees of sophistication in the subsequent calculations. Stokstad and Gross[21] numerically integrate the radial equations for many θ values, using θ-dependent radius parameters in both real and imaginary potential form factors. This procedure was deemed too time consuming in the present application, where transmission coefficients must be calculated as functions of particle type, energy, angular momentum, and deformation. Rasmussen and Sugawara-Tanabe[20] present an alternative treatment in which only the real part of the effective central potential is included (assuming a "black" nuclear interior):

$$U_{\text{eff}}^{l,\alpha_2,\theta}(r)=-\frac{V_0}{1+\exp\{[r-R(\theta)]/a_R\}}+\frac{Z_1Z_2e^2}{r}+\frac{Z_1Q_2e^2}{2r^3}P_2(\cos\theta)+\frac{\hbar^2l(l+1)}{2\mu r^2}\ . \tag{13}$$

Here $R(\theta)$ from Eq. (12) replaces the spherical real-well radius R_0, the quadrupole moment Q_2 of the target nucleus is given in terms of α_2 in the Appendix, and μ is the reduced mass. The barrier in $U_{\text{eff}}(r)$ is furthermore approximated by a parabola, leading to the following (Hill-Wheeler[33]) analytical expression for the angle-dependent transmission coefficient:

$$T_\nu^l(\epsilon,\alpha_2,\theta)=\{1+\exp[2\pi(\epsilon-B_{l,\alpha_2,\theta})/\hbar\omega_{l,\alpha_2,\theta}]\}^{-1}\ , \tag{14}$$

where $B_{l,\alpha_2,\theta}$ is the value of $U_{\text{eff}}^{l,\alpha_2,\theta}(r)$ when its radial derivative vanishes, and

$$\hbar\omega_{l,\alpha_2,\theta}=\left|\frac{\hbar^2}{\mu}\frac{d^2U_{\text{eff}}^{l,\alpha_2,\theta}}{dr^2}\right|_{\text{barrier top}}^{1/2}\ . \tag{15}$$

The final effective transmission coefficient for the deformed nucleus is then obtained by angular integration of Eq. (14):

$$T_\nu^l(\epsilon,\alpha_2)=\int_{\theta=0}^{\pi/2}T_\nu^l(\epsilon,\alpha_2,\theta)\sin\theta\,d\theta\ . \tag{16}$$

The Hill-Wheeler approximation allows a much more rapid, although cruder, evaluation of the T_ν^l than does numerical integration for a complex potential. We expect that it provides a more accurate account of the *change* in transmission from a spherical to a deformed nucleus than it does of the absolute value of the transmission coefficient for either case. We have therefore used Eqs. (13)–(16) in MBEGAT to calculate not the $T_\nu^l(\epsilon,\alpha_2)$ directly, but rather an effective energy ϵ' at which the transmission through a *spherical* potential barrier would equal that for the deformed nucleus at the actual particle energy ϵ:

$$\{1+\exp[2\pi(\epsilon'-B_{l,\alpha_2=0})/\hbar\omega_{l,\alpha_2=0}]\}^{-1}=T_\nu^l(\epsilon,\alpha_2\neq0)\ . \tag{17}$$

[Whenever the spherical ($\alpha_2=0$) real potential does not exhibit a barrier (or at least an inflection point), ϵ' is set equal to ϵ.] The shift from ϵ to ϵ' reflects the (θ-dependent) change in the height and width of the real potential barrier when the target nucleus is deformed.[20,21,34] This energy shift is calculated in the code via Eq. (17) as a function of ν, l, ϵ, and α_2; representative results are shown in Fig. 1. The final calculation of particle emission widths for deformed nuclei then uses spherical OM transmission coefficients evaluated at the relevant approximate energies ϵ'. The OM coefficients for spherical $[T_\nu^l(\epsilon,\alpha_2=0)]$ and deformed $[T_\nu^l(\epsilon',\alpha_2=0)]$ nuclei are compared for several cases in Fig. 1, to illustrate the effect of the energy shift.

We find (see Fig. 1) that the energy shift $(\epsilon'-\epsilon)$ generally crosses zero where

$$T_\nu^l(\epsilon,\alpha_2=0)\simeq0.4\ ,$$

being positive for smaller and negative for larger values of ϵ. Correspondingly, the falloff in T_ν^l with decreasing energy for fixed l (or with increasing l for an energy above the Coulomb barrier) is always more diffuse for the deformed than for the spherical nucleus, but is usually centered about similar ϵ values (or l values) for the two cases. It is clear from Fig. 1 that the deformation effect grows rapidly with increasing l, and for this reason has a more pronounced influence on emission widths for α particles than for nucleons. These observations are qualitatively consistent with the results of earlier treatments[10,20,21] of deformed-nucleus barrier penetrabilities.

Earlier calculations involving approximations similar to ours have been compared with experimental results for fusion[20,21] and elastic scattering[20] of α's or heavier ions on deformed nuclei; such comparisons suggest that as long as the deformation effects on the inverse reaction cross sections are not very large, the method used in MBEGAT should account for them adequately. The "black interior" and Hill-Wheeler approximations are expected to be less valid for nucleons than for α particles (al-

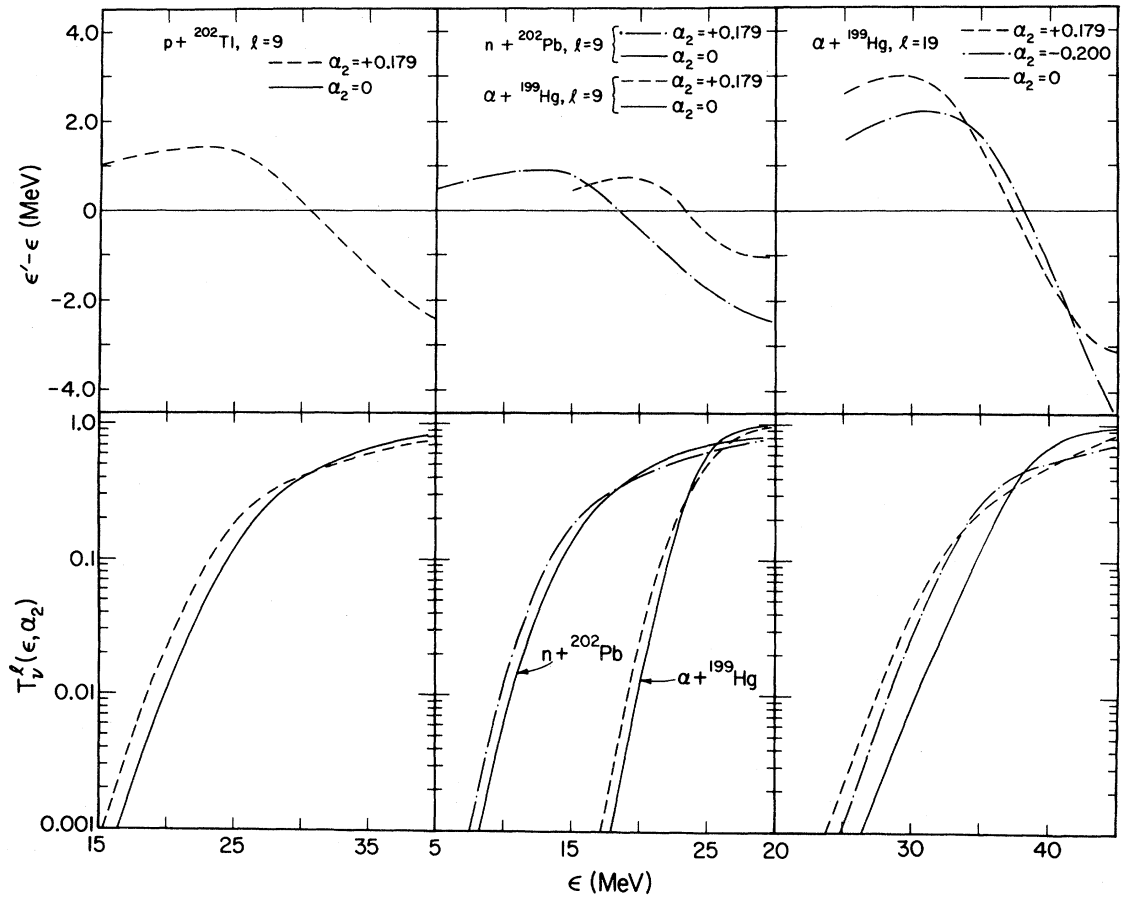

FIG. 1. Illustration for representative partial waves ($l=9$ or 19) of the deformation-induced shift in effective particle energy [$(\epsilon'-\epsilon)$ calculated with Eq. (17)], and of the associated changes in the transmission coefficients, as a function of actual particle energy ϵ for n, p, and α emission from ^{203}Pb. The broken curves are calculated following the prescription in the text for daughter nuclei with oblate ($\alpha_2<0$) or prolate ($\alpha_2>0$) deformation, as indicated in the figure, while the solid T_ν^l curves represent conventional spherical optical model results.

though probably not so bad for fusion with hot target nuclei, the processes of real interest here); but in any case, the calculated effects on nucleon emission widths are quite small.

III. COMPARISON OF CALCULATIONS FOR DIFFERENT LEVEL DENSITY TREATMENTS

A. Spherical-nucleus formalism

The evaluation of nuclear level densities in the present, as well as in most other, statistical model calculations is based on an approximate two-component Fermi-gas (NIFG) treatment,[8,24] which yields for the overall (spin-integrated) density of intrinsically excited states[35] at excitation U:

$$\Omega_{\rm intr}(U) \propto U^{-5/4}\exp[2(aU)^{1/2}] \ . \tag{18}$$

In Eq. (18) U is to be measured with respect to the ground-state energy of a nucleus *with the same deformation* as that being considered (i.e., with respect to the appropriate point on the $I=0$ PES). The level density parameter a is proportional to mass number A, with the (possibly deformation-dependent) proportionality constant generally adjusted to fit measured level densities at excitations near the neutron separation energy. Lang[19] has generalized the NIFG result to specify the density of states characterized by fixed angular momentum projection M along some chosen axis:

$$\Omega_{\rm intr}(U,M)=(2\pi\sigma^2)^{-1/2} \times\Omega_{\rm intr}[U-\hbar^2M^2/2\mathcal{I}_{\rm rig}] \ , \tag{19}$$

where $\mathscr{I}_{\rm rig}$ is the moment of inertia of a rigid body having the same density distribution with respect to the chosen axis as the Fermi gas. The "spin cutoff" parameter σ^2 is given by

$$\sigma^2 \equiv \mathscr{I}_{\rm rig}\tau/\hbar^2 , \tag{20}$$

in terms of the nuclear temperature

$$\tau \equiv \left\{ \frac{\partial}{\partial E}[\ln\Omega(E)] \right\}^{-1} . \tag{21}$$

In most of the widely used statistical model codes,[4–6,36,37] the transition from Eq. (19) to the dependence of the level density on *total* angular momentum I is made via the following relation[8,18,24]:

$$\begin{aligned}\rho(U,I) &= \Omega_{\rm intr}(U,M=I) \\ &\quad -\Omega_{\rm intr}(U,M=I+1) \\ &\simeq -\left[\frac{\partial\Omega_{\rm intr}(U,M)}{\partial M} \right]_{M=I+1/2} \\ &\simeq (2I+1)(8\pi)^{-1/2}\sigma^{-3} \\ &\quad \times \Omega_{\rm intr}\left[U - \frac{\hbar^2 I(I+1)}{2\mathscr{I}_{\rm rig}} \right] .\end{aligned} \tag{22}$$

The initial step in Eq. (22) depends on the assumption that for given I all possible projection quantum numbers, $-I \le M \le I$, are equally probable—i.e., Eq. (22) *assumes spherical symmetry.* It is the failure of this premise for any body-fixed axis in a deformed nucleus—specifically, for the saddle-point and yrast shapes relevant to high-spin decay processes—which has stimulated the present investigation of more appropriate formalisms.

In a self-consistent (albeit inappropriate) treatment via Eq. (22), the moment of inertia appearing in the argument of $\Omega_{\rm intr}$ and in the factor σ^{-3} would have to be assigned the *same* value (corresponding to a spherically symmetric matter density distribution) in evaluating level densities relevant to fission *and* to particle emission. However, one would then be unable to account for the spin dependence of the fission probability, since the decreasing fission barrier with increasing angular momentum[22] is manifested in the phase space calculations precisely through the difference between the saddle-point and the yrast rotational energy terms in the argument of $\Omega_{\rm intr}$. It is thus conventional to interpret the argument

$$U' \equiv U - \hbar^2 I(I+1)/2\mathscr{I}_{\rm rig} \simeq a\tau^2$$

as the net excitation energy of the nucleus above the PES for the appropriate *spin and shape.* In such a "hybrid" level density treatment, based on spherical symmetry but acknowledging some deformation effects, it is unclear whether one should further incorporate the moment of inertia difference in the σ^{-3} factor in Eq. (22): This difference is included in the code GROGIF (Ref. 6), but is not in MB-II (Ref. 4) or ALICE (Ref. 5). Our intention here is not to establish a preference for one or another of these codes, but rather to stress the inconsistency inherent in all of them. For simplicity, we will then compare our deformed-nucleus treatments with calculations based on only one of these "hybrid" spherical approaches, namely, that of Refs. 4 and 5; the level densities appearing in Eqs. (1) and (2) are then given by

$$\rho_f^{\rm sph}(E^*,I) \propto (2I+1)U_{\rm sad}{}^{-2} \times \exp[2(a_f U_{\rm sad})^{1/2}] , \tag{23}$$

$$\rho_\nu^{\rm sph}(E^*,J) \propto (2J+1)U_{\rm yr}{}^{-2} \times \exp[2(a_\nu U_{\rm yr})^{1/2}] , \tag{24}$$

where

$$U_{\rm sad} \equiv E^* - E_{\rm sad}(I); \quad U_{\rm yr} \equiv E^* - E_{\rm yr}(J) , \tag{25}$$

and we have allowed for different level density parameters for fission (a_f) and particle emission (a_ν). In the approach of Ref. 6, the level density ratio ρ_f/ρ_ν would be reduced from that given by Eqs. (23) and (24) by an effective factor of $(\mathscr{I}_{\rm yr}/\mathscr{I}_{\rm sad})^{3/2}$; this factor typically has a value $\simeq 0.2$ for the cases we consider in the present paper.

Calculations of fission decay widths, cross sections, and anisotropies, and of α-emission cross sections, employing the level density treatment of Eqs. (23) and (24) are represented by dashed curves in Figs. 2 and 3. The results are extremely sensitive to the ratio a_f/a_ν and slightly sensitive to the absolute value chosen for a_ν.[16] In all of the calculations reported in this paper for ^{6}Li+^{197}Au, we have used the fixed values $a_f/a_\nu = 1.039$ (based on RLDM-NIFG arguments, see the preceding paper[16]) and $a_\nu = A/9.0$ (based on smoothed shell-model single-particle level spectra in the Pb region, Refs. 38 and 39). The saddle-point and yrast energies are taken from the RLDM calculations in Ref. 22.

B. Deformed-nucleus level densities with full rotational enhancement

In the mass and spin range investigated here, the RLDM predicts[22] axially symmetric yrast and

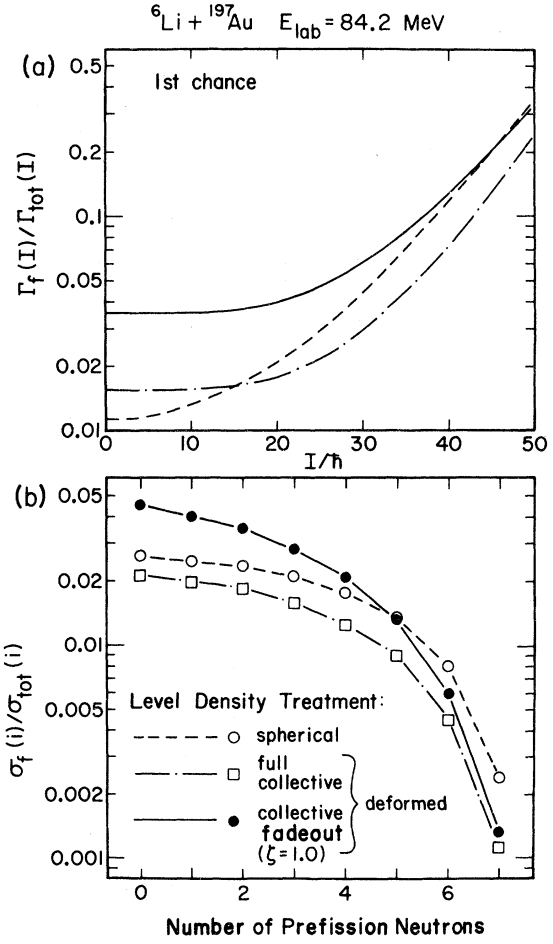

FIG. 2. The (a) spin and (b) chance distributions for fission following fusion of 84.2 MeV ^{6}Li+^{197}Au, from statistical model calculations employing the three different level density treatments outlined in Sec. III of the text. The relative partial width for 1st-chance fission is plotted versus the compound-nucleus angular momentum in (a), while the spin-integrated relative fission cross section is plotted for the various stages of the decay chain in (b). With the exception of the parameter ζ, which is introduced in allowing for the collective enhancement fadeout [see Eq. (44)], all input parameters are identical for the three calculations, with values given and justified in Ref. 16.

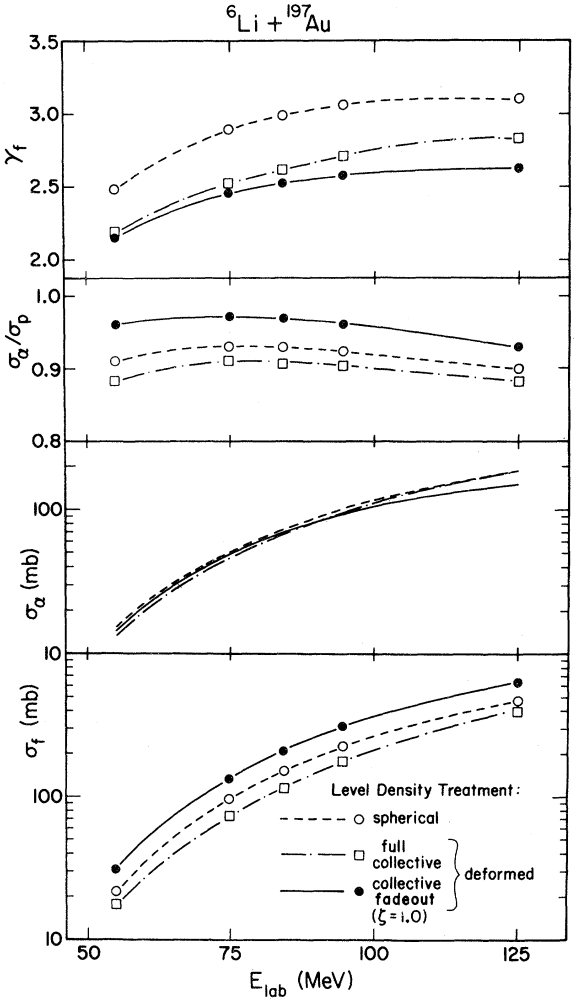

FIG. 3. The influence of the level density treatment on calculated decay properties for ^{6}Li+^{197}Au as a function of bombarding energy. The quantities displayed are the total fission cross section (σ_f) and anisotropy (γ_f), the absolute cross section for α evaporation (σ_α), and its ratio (σ_α/σ_p) to that for proton evaporation. The initial compound-nucleus spin distribution is based (Ref. 16) on an assumed total fusion cross section of 1100 mb at E_{lab}=55 MeV and 1213 mb [an average of measured values (Ref. 16) for various targets and energies] at all higher energies.

saddle-point deformations. For such nuclei it is appropriate[17,18] to apply Eq. (19) to deduce the distribution of states with respect to the (intrinsic) angular momentum projection K along the symmetry axis, and then to sum over all relevant K values to obtain $\rho(E^*,I)$, rather than using the "difference" method of Eq. (22). In doing so we are forced to address the important contribution of collective rotational bands to the density of levels at low excitation in deformed nuclei. The collective rotations do themselves arise from coherent superpositions of particle-hole excitations, which would *eventually* be counted in Ω_{intr}, but the collectivity gives them energies much lower than the unperturbed values characteristic of the contributing intrinsic states. There is consequently a collective enhancement of the level densities, at least at low temperature, which should be explicitly incorporated in the sum-

mation of states over K. This can be done as prescribed by Bjørnholm, Bohr, and Mottelson (BBM) (Ref. 18), replacing Eq. (22) with:

$$\rho(U,I)=\tfrac{1}{2}\sum_{K=-I}^{I}\Omega_{\rm intr}[U-E_{\rm rot}(I,K),K]$$
$$=(8\pi)^{-1/2}{\sigma_K}^{-1}$$
$$\times\sum_{K=-I}^{I}\Omega_{\rm intr}\left\{U-\frac{\hbar^2[I(I+1)-K^2]}{2\mathscr{I}_\perp}-\frac{\hbar^2K^2}{2\mathscr{I}_{||}}\right\}, \tag{26}$$

where ${\sigma_K}^2\equiv\mathscr{I}_{||}\tau/\hbar^2$. In Eq. (26), $[U-E_{\rm rot}(I,K)]$ is the energy of an intrinsic configuration with angular momentum projection K, upon which a collective level of total excitation U (with respect to the $I=0$ PES) and total angular momentum I is built. The factor $\frac{1}{2}$ preceding the first summation in Eq. (26) accounts for the reduction in states (restriction to non-negative K values) associated with the assumed reflection ($\mathscr{R}$-) symmetry of the nucleus.

In this subsection we describe calculations which include, via Eq. (26), the collective enhancement at low and high temperatures alike, for both the yrast and saddle-point deformations (similar calculations are included in Ref. 7). We postpone until the following subsection discussion of the possible shortcomings of this approach, particularly the double counting which is inevitable at high temperatures when $\Omega_{\rm intr}$ includes significant contributions from configurations implicitly exhausted by the lower-lying collective levels.

In relating the argument of $\Omega_{\rm intr}$ in Eq. (26) to the net excitation energies $U_{\rm sad}$ and $U_{\rm yr}$ defined by Eq. (25), we take explicit account of the expected difference in the nature of the two deformations in the mass and spin region of interest here. According to the RLDM, the saddle point on the PES for given I corresponds to a strong prolate deformation, with the angular momentum vector perpendicular to the symmetry axis, so that the rotational contribution to $E_{\rm sad}(I)$ is

$$E^{\rm rot}_{\rm sad}(I)=\hbar^2I(I+1)/2(\mathscr{I}_\perp)_{\rm sad}\ . \tag{27}$$

In contrast, the RLDM yrast deformation is mild and *oblate*, with spin *parallel* to the symmetry axis, yielding

$$E^{\rm rot}_{\rm yr}(J)=\frac{\hbar^2J(J+1)}{2(\mathscr{I}_{||})_{\rm yr}}$$
$$=\frac{\hbar^2J(J+1)}{2(\mathscr{I}_\perp)_{\rm yr}}+\frac{\hbar^2J(J+1)}{2(\mathscr{I}_{\rm eff})_{\rm yr}}\ , \tag{28}$$

where the effective moment of inertia,

$$\mathscr{I}_{\rm eff}\equiv\mathscr{I}_\perp\mathscr{I}_{||}/(\mathscr{I}_\perp-\mathscr{I}_{||})\ , \tag{29}$$

is negative for oblate and positive for prolate shapes. [It should be noted that for a Fermi gas, the simple collective rotational energy formula (28) is a good approximation to the average yrast behavior, *despite* the fact that collective rotations about a symmetry axis are strictly disallowed in a quantal treatment.[19,24]] While we assume spin along the symmetry axis for the yrast level itself, the collective excited levels to be included in ρ_ν via Eq. (26) are still those corresponding to rotations about an axis *orthogonal* to the symmetry axis. The following level density treatment, based on the distinction between Eqs. (27) and (28), becomes invalid for angular momenta just below the critical value ($I_{\rm crit}\simeq 83\hbar$ for ^{203}Pb) where the difference between yrast and saddle-point deformations, and hence the fission barrier, vanish. In that limit, of course, one should use the same form for ρ_f and ρ_ν.

Combining Eqs. (27) and (28) with Eq. (26), we obtain:

$$\rho_f^{\rm def}(E^*,I)=\hbar[8\pi(\mathscr{I}_{||})_{\rm sad}\tau_{\rm sad}]^{-1/2}\sum_{K=-I}^{I}\Omega_{\rm intr}\left[U_{\rm sad}-\frac{\hbar^2K^2}{2(\mathscr{I}_{\rm eff})_{\rm sad}}\right]; \tag{30}$$

$$\rho_\nu^{\rm def}(E^*,J)=\hbar[8\pi(\mathscr{I}_{||})_{\rm yr}\tau_{\rm yr}]^{-1/2}\sum_{K=-J}^{J}\Omega_{\rm intr}\left\{U_{\rm yr}-\frac{\hbar^2[J(J+1)-K^2]}{2\,|\,\mathscr{I}_{\rm eff}\,|_{\rm yr}}\right\}. \tag{31}$$

Note that as a result of the difference in deformations, the K distribution of the state densities peaks at $K=0$ for the saddle-point but at $|K|=J$ for the yrast shape. Substantial computing time can be saved and little accuracy lost if the summations over K in Eqs. (30) and (31) are replaced by integrals, and the integrals in turn evaluated assuming the arguments of $\Omega_{\rm intr}$ to be close to $U_{\rm sad}$ and $U_{\rm yr}$, respectively; e.g.,

$$\sum_{K=-I}^{I}\Omega_{\rm intr}\left[U_{\rm sad}-\frac{\hbar^2K^2}{2(\mathscr{I}_{\rm eff})_{\rm sad}}\right]\simeq\Omega_{\rm intr}(U_{\rm sad})\int_{-(I+1/2)}^{(I+1/2)}\exp(-K^2/2{K_0}_{\rm sad}^2)dK\ . \tag{32}$$

In Eq. (32) we have made the same Gaussian approximation to the K distribution introduced earlier [Eq. (6)] for the fission angular distribution calculation. If a power series expansion of the exponential argument in Eq. (32) were extended to include the next term

$$(-K^4\tau_{\rm sad}/16K_{0_{\rm sad}}{}^4U_{\rm sad}) ,$$

the integrand would begin to deviate noticeably from a Gaussian for $|K| \gtrsim 2K_0$, but the value of the integral in the cases of interest would not be altered by more than a couple of percent.

The approximate formulas we have actually used to evaluate the deformed-nucleus level densities in MBEGAT are as follows:

$$\rho_f^{\rm def}(E^*,I) \propto [2\pi/(\mathscr{I}_{||})_{\rm sad}]^{1/2}K_{0_{\rm sad}}{\rm erf}\left[\frac{I+1/2}{\sqrt{2}K_{0_{\rm sad}}}\right]\frac{\exp[2(a_fU_{\rm sad})^{1/2}]}{U_{\rm sad}^{3/2}} ; \tag{33}$$

$$\rho_\nu^{\rm def}(E^*,J) \propto (2J+1)(\mathscr{I}_{||})_{\rm yr}^{-1/2}\left[1-\frac{J(J+1)}{3K_{0_{\rm yr}}{}^2}+\frac{J^2(J+1)^2}{15K_{0_{\rm yr}}{}^4}\right]\frac{\exp[2(a_\nu U_{\rm yr})^{1/2}]}{U_{\rm yr}^{3/2}} , \tag{34}$$

where

$$K_0{}^2 \equiv |\mathscr{I}_{\rm eff}|\tau/\hbar^2, \quad \tau \simeq (U/a)^{1/2} , \tag{35}$$

and

$${\rm erf}(x) \equiv 2\pi^{-1/2}\int_0^x \exp(-t^2)dt . \tag{36}$$

In the approximation for ρ_ν we have taken advantage of the fact that the mild yrast deformation results in large values of $K_{0_{\rm yr}}{}^2$: Typically, in the cases considered here,

$$K_{0_{\rm yr}}{}^2 \gtrsim (1000\ {\rm MeV}^{-1})\tau_{\rm yr} ,$$

while

$$K_{0_{\rm sad}}{}^2 \sim (60\ {\rm MeV}^{-1})\tau_{\rm sad} .$$

The factors multiplying $\Omega_{\rm intr}(U)$ in Eqs. (33) and (34) vary much more slowly with excitation energy than does $\Omega_{\rm intr}$ itself; these slowly varying factors are evaluated in the code only for $E_k=0$ and $\epsilon=0$, and are removed from the integrals over these variables in Eqs. (1) and (2). RLDM values[22] for the moments of inertia $(\mathscr{I}_{||})_{\rm yr}$, $(\mathscr{I}_{\perp})_{\rm yr}$, $(\mathscr{I}_{||})_{\rm sad}$, and $(\mathscr{I}_{\perp})_{\rm sad}$ are calculated as a function of spin for each nuclide in the decay chain. The accuracy of the various approximations used in MBEGAT for numerical convenience in evaluating the deformed level densities is very good in comparison with remaining theoretical uncertainties in the formalism (see Sec. III C).

Calculations utilizing Eqs. (33) and (34) for the level densities are displayed as dashed-dotted curves in Figs. 2 and 3. It is clear from Fig. 2 that both the spin and chance distributions for the calculated fission cross section are significantly affected by replacing the spherical-nucleus with the deformed-nucleus treatment. The more rapid explicit spin dependence of ρ_ν, compared to ρ_f, in Eqs. (33) and (34) is reflected in Fig. 2(a) by an enhancement of $\Gamma_f/\Gamma_{\rm tot}$ at low spins and a suppression at high spins (and hence a decrease in the mean spin of the fissioning nuclei) in the deformed-nucleus treatment. As a result, the relative partial width for fission does not begin to increase rapidly until we have passed $I \simeq 20\hbar$. When the results in Fig. 2(a) are integrated over the full CN spin distribution, we find an overall reduction of $\sim 20\%$ in the first-chance fission cross section calculated with Eqs. (33) and (34). As seen in Fig. 2(b) this reduction factor increases to $\simeq 2$ at the late chances, resulting in an increase in the mean temperature of the fissioning nuclei, in comparison with the spherical level density treatment. The overall effect of the deformed level density treatment for 84 MeV ^{6}Li+^{197}Au is to reduce σ_f by $\sim 30\%$ and the anisotropy γ_f by $\sim 10\%$. Both the decrease in mean spin and the increase in mean temperature of the fissioning nuclei act to reduce γ_f (see Sec. II B). The comparison of calculations in Fig. 3 shows that these reduction factors depend quite weakly on bombarding energy, and that there is almost no effect on σ_α of the change from Eqs. (23) and (24) to (33) and (34).

It should be understood that the deformation has a very much larger effect on the *absolute* values of the level densities than it does on the ratio ρ_f/ρ_ν which is reflected in the calculations in Fig. 2. Comparison of Eqs. (26) and (22) in the low-spin limit yields

$$\frac{\rho^{\rm def}}{\rho^{\rm sph}} \underset{I\to 0}{\rightarrow} \frac{\sigma_K{}^{-1}}{\sigma_{\rm sph}{}^{-3}} = \left[\frac{\mathscr{I}_{\rm sph}}{\mathscr{I}_{||}}\right]^{1/2}\frac{\mathscr{I}_{\rm sph}\tau}{\hbar^2} . \tag{37}$$

For nuclei with $A \simeq 200$, $\mathscr{I}_{\rm sph}/\hbar^2 \simeq 100\ {\rm MeV}^{-1}$, so

that at the nuclear temperatures considered in the present calculations ($\tau \lesssim 2$ MeV) the deformation typically increases the abolute level density by *two orders of magnitude.* In contrast, the fission-to-particle emission ratio increases only by a factor

$$\frac{\rho_f^{\text{def}}/\rho_\nu^{\text{def}}}{\rho_f^{\text{sph}}/\rho_\nu^{\text{sph}}} \underset{I\to 0}{\to} [(\mathscr{I}_{||})_{\text{yr}}/(\mathscr{I}_{||})_{\text{sad}}]^{1/2} , \tag{38}$$

which has a value $\simeq 1.4$ for $^6\text{Li}+^{197}\text{Au}$, as seen at low spin in Fig. 2(a). The large change in absolute value results primarily from the introduction of the rotational levels, which multiplies the level density by $\mathscr{I}_\perp \tau/\hbar^2$ (approximately, the number of levels in each band with rotational energy smaller than τ, see Refs. 8, 13, 17, and 18). This collective enhancement factor is typically three times larger at the saddle-point than at the yrast deformation in our cases. Consequently, if the rotational levels had *not* been included in Eq. (26), the absolute values of ρ_f and ρ_ν would be much closer to those from Eqs. (23) and (24), but the calculated total fission cross section would be reduced by a factor ($\simeq 4$) significantly greater than that observed in Figs. 2 and 3.

C. Allowance for the collective enhancement fadeout

1. *Qualitative effect of the fadeout*

The level density treatment described in the preceding subsection is at least internally consistent, and thus represents a considerable improvement over Eqs. (23) and (24). However, there are several serious concerns about the general quantitative validity of deformed-nucleus approaches based strictly on Eq. (26). For example, that equation is based on the assumption of axial and reflection symmetry; triaxial nuclei have more rotational degrees of freedom, and hence a greater collective enhancement of the level density.[18] In addition, collective *vibrational* states have not been included, since they tend to occur at significantly higher excitation than the rotational states. This neglect may be important for small deformations, as it contributes to the artificial discontinuity[18] in the state density [by a factor $\sim\sigma^2$, see Eq. (37)] as one approaches spherical symmetry and passes from Eq. (26) to Eq. (22).

Of even greater concern in the present application than the above caveats is the central assumption behind Eq. (26), that of complete independence of the collective and intrinsic degrees of freedom. In a broad sense, this assumption is not valid, since all nuclear excitations can be accounted for, in principle, by intrinsic degrees of freedom alone. However, as noted in the preceding subsection, the collectivity does act to *redistribute* levels with respect to energy, giving rise to an *effective* separation between rotational and intrinsic motion at low temperatures. As stressed by BBM,[18] this effective distinction must begin to fade at temperatures where the single-particle excitations which contribute coherently to the rotational motion would also contribute appreciably to the intrinsic level density. The relevant single-particle excitations are generated by the Coriolis coupling,[18,24] and in an axially symmetric harmonic oscillator well they fall predominantly at energies

$$\epsilon_{\text{Coriolis}} \sim \pm\hbar(\omega_2-\omega_3) \sim (41\text{ MeV})A^{-1/3}|\delta_{\text{osc}}| . \tag{39}$$

In Eq. (39), ω_2 and ω_3 denote the oscillator frequencies for particle motion in the directions perpendicular to the rotation axis; their difference can be expressed as the product of the mean oscillator frequency ($\hbar\omega_0 \simeq 41A^{-1/3}$ MeV) and a potential deformation parameter[24] δ_{osc} (positive for prolate and negative for oblate shapes).

Equations (33) and (34) are strictly applicable only at temperatures small in comparison with $\epsilon_{\text{Coriolis}}$. When $\tau \gg \epsilon_{\text{Coriolis}}$ there can no longer be any distinction between rotational and intrinsic degrees of freedom, and the appropriate (purely intrinsic) deformed-nucleus level densities can be obtained[8,40] by dividing Eqs. (33) and (34) by the collective enhancement factor $\mathscr{I}_\perp\tau/\hbar^2$ ($\sim 10^2$). In this section we describe a method for treating the *intermediate* temperature region, where there must be a *smooth transition* from the collectively enhanced to the purely intrinsic form for the level density. In a previous attempt to include such a transition in statistical model calculations,[41] the expected dependence of $\epsilon_{\text{Coriolis}}$ on δ_{osc} was effectively neglected. To see that this deformation dependence is of crucial importance in evaluating fission probabilities for hot nuclei, one need only note that RLDM shapes[22] for the nuclei investigated in the present work are typically characterized by values $\delta_{\text{osc}} \sim -0.04$, $\epsilon_{\text{Coriolis}} \sim 0.3$ MeV at the potential energy minimum, and $\delta_{\text{osc}} \sim 1.0$, $\epsilon_{\text{Coriolis}} \sim 7$ MeV at the saddle point. At temperatures $\tau \sim 1-2$ MeV, one would then expect the collective enhancement to be almost fully depleted in the yrast level densities, but still fully effective in ρ_f. At first sight, it might seem that this difference would lead to an enhancement of fission widths by about two orders

of magnitude over those calculated with Eqs. (33) and (34).

The latter inference, which suggests a temperature dependence of $\Gamma_f/\Gamma_{\rm tot}$ much more rapid than is observed,[30] is based on flawed reasoning. If at temperature τ the collective enhancement is indeed fully depleted at the RLDM yrast shape, but fully effective at the saddle point, one must expect to find a maximum value of ρ_ν at some intermediate deformation, in the vicinity of

$$|\delta_c| = \tau A^{1/3}/(41\ \text{MeV}) , \tag{40}$$

where an *almost* complete collective enhancement more than compensates for the reduction in *intrinsic* level density from the yrast value. Recall from the discussion in Sec. II A that the appropriate deformation to use in particle emission calculations (short of a complete, but excessively time-consuming, integration over deformation) is the *most probable* one reached in the daughter nucleus. A realistic (i.e., deformation-dependent) treatment of the collective enhancement fadeout thus leads naturally to a *temperature-dependent shift in the deformation at which level densities* (and barrier transmission coefficients) *are evaluated for particle emission.* The saddle-point properties are unaffected at the temperatures of interest here.

The existence of such a shift in the most probable deformation is illustrated in Fig. 4 by level density calculations for ^{202}Pb at $J=25\hbar$ employing two different, somewhat arbitrary, analytical expressions for the fadeout of the collective enhancement. We have constrained both expressions to satisfy the following criteria: (i) the collective enhancement vanishes in the limit $|\delta|/\tau \to 0$, thereby ensuring a smooth transition in ρ_ν from deformed to spherical nuclei; (ii) for a given deformation δ, the collective enhancement is complete for $\tau \ll \epsilon_{\rm Coriolis}$, and is reduced by a factor $\simeq \frac{1}{2}$ when $\tau = \epsilon_{\rm Coriolis}$. Both fadeout expressions are taken in the form

$$\rho_\nu(E^*,J,\delta) = \rho_\nu^{\rm def}(E^*,J,\delta) \times \left[1-\chi(\delta,\tau)\left[1-\frac{\hbar^2}{\mathscr{I}_\perp \tau}\right]\right] , \tag{41}$$

with $\rho_\nu^{\rm def}(E^*,J,\delta)$ calculated from Eq. (33) for $\delta>0$ and from Eq. (34) for $\delta<0$. [Equations (33) and (34) approach the same limiting form as $|\delta| \to 0$. The proportionality constant omitted from both of these equations has been set equal to $\hbar$ for the purposes of Fig. 4.] In the "slow" collective fadeout treatment (dashed curves in Fig. 4) the dilution function $\chi(\delta,\tau)$ is tied simply to the Fermi-gas occupancy of single-particle levels at energy $\hbar\omega_0|\delta|$,

$$\chi_{\rm slow}(\delta,\tau) = 2[\exp(\hbar\omega_0|\delta|/\tau)+1]^{-1} , \tag{42}$$

while the dotted-dashed curves assume a more rapid disappearance of the enhancement:

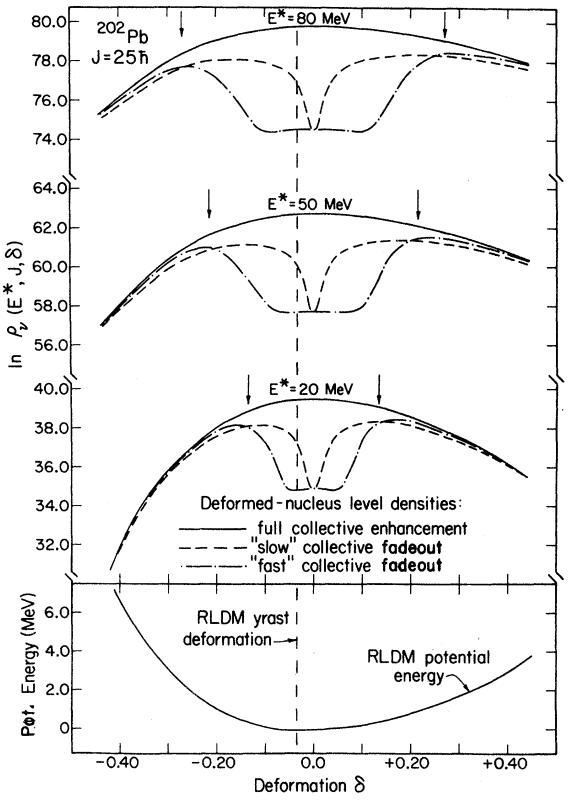

FIG. 4. Illustration of the temperature-dependent shift in the most probable daughter-nucleus deformation when the collective level density enhancement is allowed to fade as the temperature approaches the single-particle Coriolis excitation of Eq. (39). The potential energy curve in the bottom frame is calculated for axially symmetric shapes in ^{202}Pb, at an angular momentum of $25\hbar$, using the approximate relations in the Appendix and setting the energy to zero at spherical symmetry. The dashed vertical line marks the deformation corresponding to the minimum potential energy. In the top frame the logarithm of the level density is plotted versus deformation for three excitation energies. The E^* values are specified in the figure with respect to the potential energy of a rigid sphere, but in the level density calculations these values are decremented by the deformation energy for $\delta \neq 0$. The solid level density curves are calculated with Eqs. (33) and (34), and the broken curves with Eq. (41), using the dilution functions from either Eq. (42) (dashed curves) or Eq. (43) (dotted-dashed). The vertical arrows indicate the oblate and prolate shapes corresponding to the cutoff deformation of Eq. (40) for each excitation.

$$\chi_{\text{fast}}(\delta,\tau)=\{\exp[5(1-\tau/\hbar\omega_0\,|\,\delta\,|\,)]+1\}^{-1}\ . \tag{43}$$

The deformation energies (to be subtracted from E^*) and moments of inertia needed for the calculations in Fig. 4 have been evaluated as a function of δ using the relations compiled in the Appendix. We have furthermore included in these calculations a variation of the level density parameter a_ν with deformation, as prescribed by Bishop *et al.*[23] on the basis of NIFG calculations for nuclei with diffuse surface regions and deformation-dependent surface-to-volume ratios. The maximum increase in a_ν from the value assumed for spherical nuclei ($A/9.0$) is only 0.7% over the range of deformations included in Fig. 4.

The calculations in Fig. 4 demonstrate clearly that the collective enhancement fadeout results in a considerable displacement between the deformations corresponding to the maximum level density and to the minimum potential energy. At a given excitation energy, this displacement is appreciably different for the "slow" and "fast" fadeout assumptions, but in both cases it grows in rough proportionality to the temperature. Furthermore, the peak value of the level density $[\rho_\nu^{\max}(E^*,J)]$ is quite similar for the dashed and dotted-dashed curves, smaller in each case than the yrast level density including full collective enhancement [i.e., the value $\rho_\nu^{\text{def}}(E^*,J)$ used in the particle emission calculations described in Sec. III B], but very much larger than the purely intrinsic level density appropriate to spherical symmetry. Consequently, either of the fadeout treatments in Fig. 4 would lead to a suppression of particle emission relative to fission in comparison with full collective calculations, but by a factor ~ 2, rather than $\sim 10^2$ as appeared initially. This suppression factor $[\rho_\nu^{\text{def}}(E^*,J)/\rho_\nu^{\max}(E^*,J)]$ increases slowly as the most probable deformation shifts further away from the RLDM yrast value ($\delta_{\text{yr}}^{\text{RLDM}}$), i.e., as the temperature increases for fixed spin of the daughter nucleus, or as the spin (and hence $|\,\delta_{\text{yr}}^{\text{RLDM}}\,|$) decreases for fixed τ.

2. *Incorporation in the code*

Expressions (41)–(43), and the calculations based on them, have been introduced here for illustrative purposes only. The actual treatment of the collective enhancement fadeout in MBEGAT is (for computational convenience) more simplistic than those in Fig. 4, but it adequately incorporates all of the important features discussed above. In the code we use the *collectively enhanced* level densities for particle emission, but we evaluate them (as well as the transmission coefficients T_ν^l, see Sec. II C) at an effective deformation equal to the larger of the RLDM yrast value ($|\,\delta_{\text{yr}}^{\text{RLDM}}\,|$) and

$$|\,\delta_{\text{eff}}\,| = \tau A^{1/3}/(41\zeta\ \text{MeV})\ , \tag{44}$$

where ζ is an adjustable normalization factor, independent of J and E^*. For each E^*-J bin where $|\,\delta_{\text{eff}}\,|$ exceeds $|\,\delta_{\text{yr}}^{\text{RLDM}}\,|$, the level density is evaluated both at $+|\,\delta_{\text{eff}}\,|$, using Eq. (33), and at $-|\,\delta_{\text{eff}}\,|$ via Eq. (34), with the larger of the two resulting ρ_ν values used to determine the emission widths. For example, if ζ were chosen to be unity, then for each excitation energy considered in Fig. 4 we would take ρ_ν from the values of the *solid* level density curve at the two deformations marked by the vertical arrows; the larger of these two values of ρ_ν would be used in the decay calculations. This procedure is based strictly on the assumption of a sharp cutoff in the rotational levels within each E^*-J bin at the associated value of $|\,\delta_{\text{eff}}\,|$; however, the effect of this cutoff varies smoothly with E^* and J, in a manner quite similar to that expected of more sophisticated treatments springing from Eq. (39). The introduction of the normalization factor ζ provides some freedom to accommodate the quantitative uncertainties which exist in the precise location of the relevant Coriolis excitations and in their precise relation to the temperature scale characterizing the reduction in the collective enhancement. While ζ should certainly be of order unity, it is appropriate to investigate the influence on statistical model calculations of plausible variations in this parameter.

Some representative features of calculations incorporating the above "sharp cutoff" of the collective enhancement are displayed in Fig. 5. In the top part we have plotted the effective deformation (for $\zeta=1.0$) as a function of spin (I) for two stages in the decay of ^{203}Pb formed in 125 MeV ^{6}Li fusion with ^{197}Au. Rather than δ, we have plotted the related quantity α_2 [see Eq. (A2)], the quadrupole deformation coefficient introduced in Eq. (12). Also included in Fig. 5(a) for comparison is an estimate of $\alpha_2^{\text{yrast}}(I)$ for the RLDM yrast shape, based on Eq. (A15). The most probable deformations in the hot nuclei tend to be prolate at low angular momenta, despite the mild oblate deformation at the potential energy minimum, because the PES rises less steeply on the prolate side (see Fig. 4). At high spin a discontinuous transition to oblate most probable

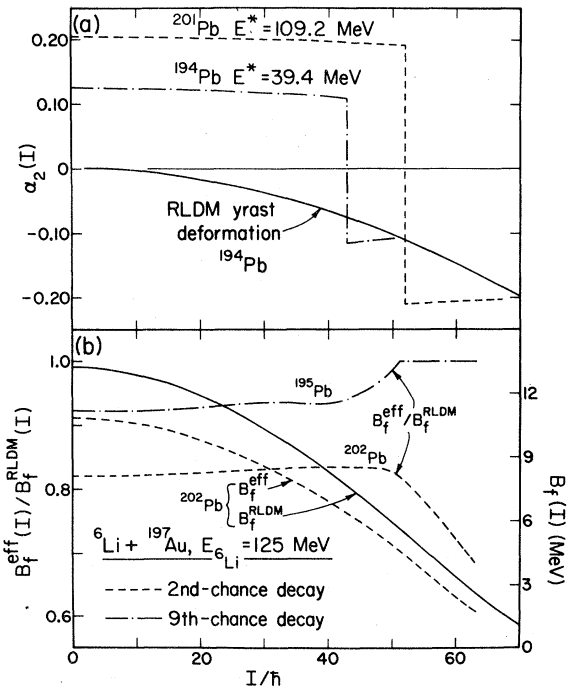

FIG. 5. The broken curves represent the spin dependence of (a) the daughter-nucleus deformation used for 0.1 MeV neutron emission and (b) the corresponding effective fission barrier height [see Eq. (46)] relevant to calculations incorporating the fadeout of the collective level density enhancement, for two stages in the decay of ^{203}Pb following fusion of 125 MeV ^{6}Li+^{197}Au. For comparison, the solid curves display representative RLDM results, for (a) the yrast deformation in ^{194}Pb (the RLDM values in ^{201}Pb would be lower in magnitude by $\sim$12%), and (b) the fission barrier in ^{202}Pb (the RLDM values for ^{195}Pb would be lower by a spin-dependent factor, $\sim$11% for $I=0$ and $\sim$25% for $I=50\hbar$). When the RLDM yrast deformation exceeds the collective cutoff values (as for $I>51\hbar$ at 9th chance), conventional RLDM predictions are used for all relevant nuclear structure properties.

shapes occurs in the calculations, when the potential energy minimum has progressed to deformations almost as large in magnitude as the cutoff deformation. At the lower excitation considered in Fig. 5(a), the RLDM yrast deformation exceeds the cutoff value, and hence is used in its place to evaluate particle emission widths, for $I>51\hbar$; the corresponding intersection for the higher excitation does not occur until $I\simeq 70\hbar$ (where the approximate treatment of deformation in the Appendix is already of questionable validity). It may be noted from the figure that at a fixed overall excitation energy the magnitude of the cutoff deformation decreases slowly with increasing I, reflecting the reduction of τ as an increasing fraction of E^* is exhausted by the rotational potential energy.

The primary effect of the collective enhancement cutoff on the competition between fission and particle decay may be characterized by the change from the RLDM fission barrier height

$$B_f^{\mathrm{RLDM}}(I)=E_{\mathrm{sad}}^{\mathrm{RLDM}}(I)-E_{\mathrm{yr}}^{\mathrm{RLDM}}(I) \tag{45}$$

to an effective barrier

$$B_f^{\mathrm{eff}}(I)=E_{\mathrm{sad}}^{\mathrm{RLDM}}(I)-E_{\mathrm{yr}}^{\mathrm{eff}}(I)\ , \tag{46}$$

where $E_{\mathrm{yr}}^{\mathrm{eff}}(I)$ is the potential energy at the most probable deformation. Values of the ratio $B_f^{\mathrm{eff}}/B_f^{\mathrm{RLDM}}$, corresponding to the deformation curves in Fig. 5(a), are plotted in Fig. 5(b). Both B_f^{RLDM} and B_f^{eff} decrease rapidly with increasing I, but their ratio remains roughly constant (for given E^*) over much of the spin range of interest in the present calculations. The ratio must approach unity as the shift between the RLDM yrast and most probable deformations vanishes, i.e., at low τ and high I [in the case of ^{202}Pb, Fig. 5(b), the ratio goes through a minimum just beyond the spin range shown and then rises rapidly to unity at $I\simeq 70\hbar$].

The effects of the collective enhancement fadeout which one should expect qualitatively from the preceding discussion are borne out by the comparison of calculated results in Fig. 2. Fission is clearly enhanced with respect to particle emission, by a factor which grows with increasing temperature, and for fixed temperature, with decreasing spin. The increase in the relative contributions to fission from early chances and low angular momenta reinforces the trend already observed in the replacement of the spherical [Eqs. (23) and (24)] by the full collective [Eqs. (33) and (34)] level density treatment. The changes to the I and τ dependence both act to reduce the fission anisotropy slightly, while they tend to cancel in their effects on the variation of the total fission cross section with bombarding energy (see Fig. 3).

It should be noted from Fig. 3 that the calculations incorporating the collective fadeout yield results for σ_f, γ_f, and σ_p/σ_α that do not fall between those for the spherical and full collective limits. This result is not surprising: In any fadeout prescription, the *absolute* level density at given values of E^*, J, and δ is clearly required to lie between the corresponding purely intrinsic and fully collectively enhanced densities, *but the relative level densities for different deformations or different excitations* (and hence the competition between different

decay modes) *are not similarly constrained.* Indeed, the results in Fig. 4 illustrate that the *shape* of the level density curves as a function of deformation is altered much more radically by the fadeout than by the full inclusion or full exclusion of the collective enhancement.

The magnitude of the fadeout effect on σ_f is strongly dependent on the cutoff-deformation normalization parameter ζ, as illustrated in Fig. 6. In comparison with the calculations based on the full collective level density treatment, σ_f increases by a factor $\simeq 1.4$ for $\zeta=1.3$, $\simeq 1.8$ for $\zeta=1.0$, and $\simeq 3.0$ for $\zeta=0.7$, roughly independent of the bombarding energy (except for a natural saturation when σ_f exhausts a dominant fraction of the fusion cross section). Correspondingly, γ_f for 84.2 MeV ^{6}Li+^{197}Au is lowered by 2.4%, 3.7%, or 6.8%. The fractional reduction in γ_f grows with increasing bombarding energy (see Fig. 3), but even at 125 MeV for $\zeta=0.7$ it remains $\lesssim 15\%$. The more rapid change of the fission predictions as ζ decreases from unity, in comparison with increasing ζ, reflects the steeper slope of the (solid) level density curves in Fig. 4 with greater displacement from spherical symmetry. In the absence of direct experimental information on the degree of persistence of rotational bands at high temperature, the range of ζ values considered in Fig. 6 is felt to represent a reasonable guess at the level of quantitative uncertainty in the fadeout treatment. It thus appears necessary to treat ζ as an adjustable parameter in comparisons of statistical model calculations with experimental results on the decay properties of hot, high-spin nuclei.

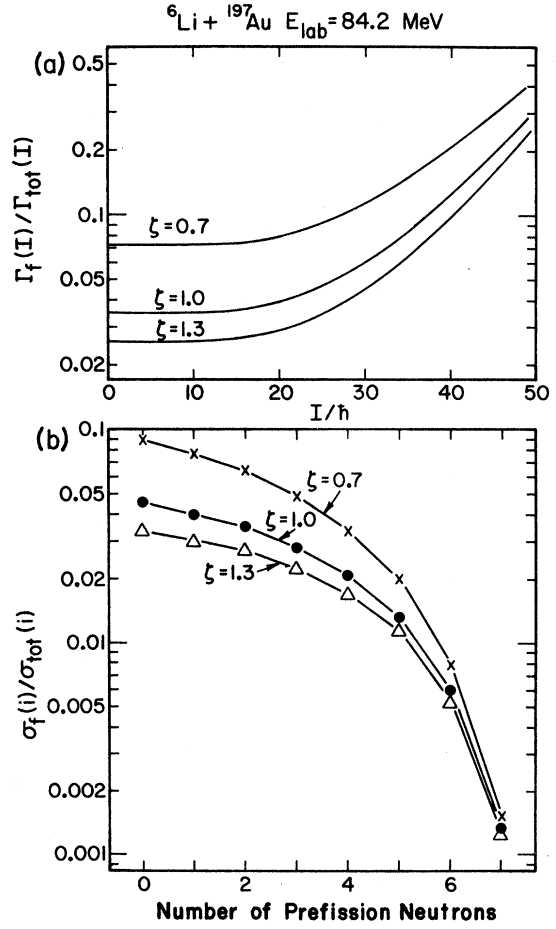

FIG. 6. As in Fig. 2, except for three calculations incorporating the collective fadeout, but with different values for the cutoff-deformation normalization parameter ζ.

Up to now, we have included the treatment outlined here in an analysis of one extensive data set, that reported for ^{6}Li-induced fusion with targets of $A\simeq 200$ in the preceding paper[16]; when all nuclear structure parameters are fixed to RLDM-NIFG predictions, and the effects of preequilibrium nucleon emission are incorporated in the calculations, very good quantitative agreement with all measured quantities is obtained with $\zeta=1.05$. However, the effects of the above level density treatment on σ_f and γ_f for a given system are not unique—they can be simulated by appropriate changes to other input parameters of the code[16]—and the effects on other calculated quantities seem unfortunately too small to serve as a signature for the collective fadeout. For example, while the increased daughter-nucleus deformation does enhance barrier transmission for α particles relative to nucleons, as expected from the discussion in Sec. II C, the resultant change in the ratio σ_α/σ_p is no more than 10% at any of the bombarding energies considered (see Fig. 3). Furthermore, the penetrability effect is counterbalanced by the increasing fission competition, so that the collective fadeout produces almost no net alteration in the *absolute* α-emission cross sections (Fig. 3). The only appreciable change in the calculated energy spectra for evaporated particles (see Fig. 7) is a slight enhancement in the yield of sub-barrier α's.

Systematic measurements which permit some separation of the spin and temperature dependences of fission probabilities would seem to offer the best hope for experimental confirmation of the deformation-dependent dilution of collective level density enhancements. Appropriate experiments might involve decay studies for a given compound nucleus formed with widely differing entrance channels, or measurements of projectile fragment-fission fragment coincidences (over a broad energy

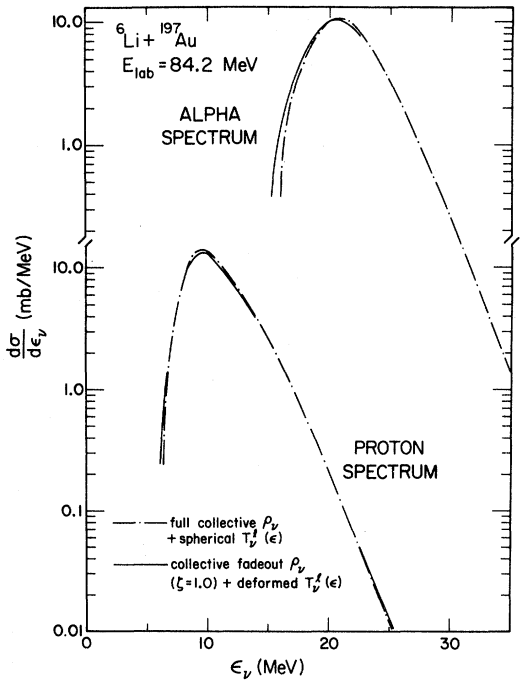

FIG. 7. Influence of the collective level density fadeout and deformed-nucleus barrier transmission on the calculated energy spectra for proton and α evaporation. Without inclusion of the deformed barrier transmission, there would be essentially no difference in shape between the solid and dotted-dashed curves.

range for the former particle) in incomplete fusion reactions. In order to illustrate the potential sensitivity of the former class of experiments, we have performed statistical model calculations, using all three of the level density treatments discussed here, for the decay of ^{202}Pb formed in fusion of ^{22}Ne+^{180}Hf at two bombarding energies. The first energy ($E_{^{22}\mathrm{Ne}}$=89 MeV) was chosen to yield a CN spin distribution similar to that obtained in ^{203}Pb from 84.2 MeV ^{6}Li+^{197}Au fusion, but at substantially lower initial temperature; at the second energy ($E_{^{22}\mathrm{Ne}}$=136 MeV) the initial temperature is the same as for the ^{6}Li+^{197}Au case, but considerably higher spins are populated. The ratios of calculated decay properties for the ^{22}Ne- vs ^{6}Li-induced fusion are listed in Table I. The most significant effect of the level density treatment is the reduction in the fission ratio $\sigma_f(^{22}\mathrm{Ne})/\sigma_f(^6\mathrm{Li})$ for both ^{22}Ne bombarding energies when the collective enhancement fadeout is included. This reduction reflects the larger contributions to the ^{22}Ne-induced fission from low temperatures (at the first bombarding energy) and from high angular momenta (at the second energy). The magnitude of the reduction seems large enough that in an analysis of careful and complete measurements it should not be masked by uncertainties in the relative fusion cross sections, or in the relative importance of preequili-

TABLE I. Ratio of calculated quantities for compound nucleus decay following ^{22}Ne+^{180}Hf fusion vs 84.2-MeV ^{6}Li+^{197}Au fusion.

^{22}Ne bombarding energy (MeV)	E^*_{CN} (MeV)	σ_{fus}[a] (mb)	$I_0/\hbar$[b]	Level density treatment	$\frac{\sigma_f(^{22}\mathrm{Ne})}{\sigma_f(^6\mathrm{Li})}$	$\frac{\gamma_f(^{22}\mathrm{Ne})}{\gamma_f(^6\mathrm{Li})}$	$\frac{\sigma_\alpha(^{22}\mathrm{Ne})}{\sigma_\alpha(^6\mathrm{Li})}$	$\frac{\sigma_p(^{22}\mathrm{Ne})}{\sigma_p(^6\mathrm{Li})}$
89.1	41.4	430	31.0[c]	spherical	0.0684	1.44	0.0288	0.0306
				full collective	0.0494	1.49	0.0264	0.0279
				collective fadeout	0.0418	1.50	0.0288	0.0292
136.2	83.4[c]	1150	63.7	spherical	5.19	1.75	0.591	0.540
				full collective	6.12	1.96	0.687	0.598
				collective fadeout	3.74	1.97	0.637	0.568

[a]Fusion cross sections for ^{22}Ne+^{180}Hf were calculated according to the prescription developed by Bass, Ref. 42.

[b]The CN angular momentum for which the partial cross section is taken to be half of the corresponding unitarity limit, i.e., $0.5\pi\lambda\!\!\!^{-2}(2I_0+1)$. For the ^{22}Ne+^{180}Hf entrance channels, the CN spin distribution has been assumed to have a Fermi-function falloff characterized by the same diffuseness value ($2.70\hbar$) as used for 84.2-MeV ^{6}Li+^{197}Au (see Ref. 16).

[c]The ^{22}Ne bombarding energy was chosen to yield approximately the same value for this quantity as used for 84.2-MeV ^{6}Li+^{197}Au.

brium particle emission, for the different entrance channels.

It should be kept in mind that the treatment we have proposed is justifiable only at nuclear temperatures sufficiently high that we may safely neglect microscopic corrections to the PES and the level densities. At lower temperatures, shell corrections may well introduce local fluctuations in deformation probability curves (e.g., see Ref. 25) which are more important than the modifications in Fig. 4 arising from the collective enhancement fadeout. In addition, for nuclei with substantial ground-state deformations, the "melting" of the shell corrections with increasing temperature[24,25,43] will lead naturally to a *decrease* in the effective yrast deformation—from the microscopically corrected toward the RLDM value—counteracting the effect illustrated in Fig. 4.

IV. CONCLUSIONS

Statistical model calculations of the decay properties of hot, high-spin nuclei depend on the *relative* level densities appropriate to different decay modes, and they do not, in general, require as much sophistication as treatments aimed at reproducing measured *absolute* level densities at relatively low excitation.[11–15] Nonetheless, the evaluation of level densities in most existing statistical model codes seems needlessly crude in several respects, especially in the incorporation of deformation effects. In the present paper, we have compared calculations of decay properties based on three different approaches to evaluating level densities as a function of excitation energy and angular momentum: (1) an internally inconsistent, but widely used, treatment which implicitly assumes spherical symmetry of the nucleus; (2) a formalism appropriate to deformed nuclei, but assuming a complete independence of rotational and intrinsic degrees of freedom at all deformations and temperatures; and (3) a modification to method (2) allowing for the expected dilution of rotational band structure at high excitation. In order to simplify the calculation and discussion of deformation effects, we have systematically ignored the influence of shell and pairing corrections to the level densities in all three approaches, as should become appropriate at moderately high temperature.[16,24,25,39] We have thus implicitly assumed that (at sufficiently large deformation) collective bands may continue to enhance level densities even after microscopic structure corrections are washed out; this assumption is experimentally untested and subject to question.

Method (2) for incorporating the full collective enhancement is well established theoretically,[17,18] and has been reasonably successful in accounting for measured level densities at low excitation in deformed nuclei.[13,14] The effects are much smaller for relative than for absolute level densities, but they result in appreciable changes to calculated fission cross sections and anisotropies (see Figs. 2 and 3). Our technique for including the fadeout of the collective enhancement with increasing temperature is more speculative, and is appropriate only at temperatures considerably higher than those accessible in direct level density measurements. As long as one starts from the theoretical expectation[18,24] that the temperature characteristic of this fadeout increases in proportion to the nuclear deformation (and is substantially larger at the saddle point than the temperature from which the decay begins), then the qualitative effects on statistical model calculations can be surmised independent of computational details: The most probable deformation reached in particle emission will increase progressively with increasing temperature, and the relevant level density will correspondingly decrease, from the values associated with the minimum in the potential energy surface and full collective enhancement; fission will be enhanced with respect to particle emission, with the largest effects at low angular momenta and high temperatures. In our treatment an adjustable normalization parameter ζ for the deformation shift is introduced to accommodate quantitative uncertainties in the theory of the collective fadeout. The fission enhancement factor produced by the fadeout is quite sensitive to ζ, varying for the system considered in the present calculations from ~ 1.5 to ~ 3.0 for different plausible choices of this parameter. The quantitative effect of the fadeout is thus quite uncertain, but perhaps our most important conclusion is that it, like the effect of the inclusion of collective bands in the first place, is much *smaller* than the associated order of magnitude changes in absolute level densities.

The net effect of the change from level density treatment (1) to (3) above for the $^{6}\mathrm{Li}+^{197}\mathrm{Au}$ system is a moderate increase ($\sim 50\%$) in the fission cross section σ_f and a reduction ($\sim 15\%$) in the fission anisotropy γ_f, with little change in the bombarding energy dependence of these quantities. A slight ($\sim 5\%$) enhancement of α particle relative to nucleon evaporation arises from the influence of the increased daughter-nucleus deformation on barrier transmission coefficients. While treatment (3) is to be preferred on theoretical grounds, there is little

hope of providing convincing experimental support for this preference by comparing statistical model calculations with measurements of quantities (such as σ_f and γ_f) that are integrated over the angular momentum and excitation energy distributions of the decaying nuclei. Rather, we encourage experiments aimed at mapping out the spin and temperature dependences of fission probabilities as a means for confirming the existence, and constraining the magnitude, of the temperature-dependent shift in the most probable deformation which accompanies the collective enhancement fadeout in our level density treatment.

ACKNOWLEDGMENTS

We are grateful to Dr. J. M. Alexander, Dr. M. Beckerman, Dr. M. Blann, and Dr. R. G. Stokstad for helpful discussions concerning various aspects of statistical model analyses, and to Dr. P. P. Singh for his careful reading of the manuscript. We also thank Dr. Beckerman and Dr. Blann for providing us with a version of their code MB-II, to which we have added the features described in this and the preceding paper. The fission-fragment angular distribution calculation was incorporated with the help of Mr. P. Yip. Our work was supported in part by the National Science Foundation.

APPENDIX: DEFORMATION-DEPENDENCE OF NUCLEAR STRUCTURE PROPERTIES NEEDED IN THE COLLECTIVE ENHANCEMENT FADEOUT TREATMENT

The evaluation of level densities in the statistical model code MBEGAT requires calculation of the deformation energy and moments of inertia for nuclei of various shapes. In the level density treatments outlined in Secs. III A and III B, and for the fission level densities involved in the calculations described in Sec. III C, the shapes of interest always represent a minimum or saddle point of a RLDM potential energy surface; in these cases the relevant energies and moments of inertia are taken directly from the published results of Cohen, Plasil, and Swiatecki.[22] In allowing for the fadeout of the collective enhancement, however, we evaluate the level densities ρ_ν for particle emission, according to Eqs. (33) or (34), at "effective yrast" deformations which generally deviate considerably from the corresponding RLDM shapes. In this appendix we give the relations used in MBEGAT to compute the structure properties needed in evaluating ρ_ν, and also the transmission coefficients $T_\nu^l(\epsilon)$, for these "effective yrast" shapes.

The effective shape is defined by Eq. (44) in terms of the deformation parameter[24] δ for an axially symmetric harmonic oscillator potential. For the purposes of computing energies and moments of inertia it is more convenient to work with the quadrupole matter deformation parameter α_2 appearing in a Legendre polynomial expansion of the surface contour for an axially and reflection-symmetric nucleus:

$$R(\theta)=R_0[\,1+\alpha_0+\alpha_2 P_2(\cos\theta) +\alpha_4 P_4(\cos\theta)+\cdots\,]\,. \tag{A1}$$

Assuming α_2 to be by far the largest of the α coefficients in this expansion, we obtain α_2 from δ via their respective relationships[24] to the length ratio r of the symmetry axis to the orthogonal axes:

$$r^2=(4\delta+3)/(3-2\delta)\,;$$
$$\alpha_2=(r-1)/(1+r/2)\,. \tag{A2}$$

The effective deformations considered in the calculations are almost always small enough to warrant truncation of the expansion (A1) at the P_4 term. The coefficient α_0 is constrained to ensure equality of the volumes of the deformed nucleus and of the corresponding spherical nucleus of radius R_0. Through order α_2^4 and α_4^2 this constraint yields:

$$\alpha_0=-0.2\alpha_2^2-0.019\alpha_2^3-0.057\alpha_2^2\alpha_4-0.111\alpha_4^2\,. \tag{A3}$$

The hexadecapole deformation coefficient α_4 is adjusted for given α_2 to minimize the total (Coulomb plus surface plus rotational) potential energy of the deformed rotating nucleus, which can be characterized by fissility[22]

$$x=0.01965\eta^{-1}Z^2A^{-1} \tag{A4}$$

and angular momentum parameter[22]

$$y=1.9249\eta^{-1}I(I+1)A^{-7/3}\,, \tag{A5}$$

where I is the angular momentum and η is the neutron-proton difference term

$$\eta = 1 - 1.7826(N-Z)^2 A^{-2} . \quad \text{(A6)}$$

The minimization procedure [based on Eqs. (A10), (A13), and (A14) below] gives

$$\alpha_4 = (1 - 0.370x - c_1 y)^{-1} \times [\alpha_2^2(0.057 + 0.171x + c_2 y) + c_3 \alpha_2 y] , \quad \text{(A7)}$$

with

$$c_1 = -0.266 , \quad c_2 = -0.896 , \quad c_3 = -0.571 \quad \text{(A8)}$$

for $\alpha_2 < 0$ and

$$c_1 = -0.700 , \quad c_2 = 0.663 , \quad c_3 = 0.286 \quad \text{(A9)}$$

for $\alpha_2 > 0$, for oblate and prolate deformations, respectively. For the calculations presented in this paper, typical values for the above parameters are $x \simeq 0.70$, $y \lesssim 0.010$, $-0.2 \lesssim \alpha_2 \lesssim 0.2$, $0 < \alpha_4 \lesssim 0.01$, and $-0.01 \lesssim \alpha_0 < 0$.

The deformation energy and moments of inertia are computed through fourth order in the quadrupole and second order in the hexadecapole coefficients. The expansion for the liquid-drop potential energy E, relative to the energy $E^{(0)}$ for a rotating *sphere* characterized by x and y, is adapted from Swiatecki[44]:

$$E - E^{(0)} = E^{(0)}_{\text{surf}} \left\{ \alpha_2^2[0.4(1-x)] - \alpha_2^3[0.038(1+2x)] - \alpha_2^4[0.217 - 0.256x] - \alpha_2^2\alpha_4[0.114(1+3x)] + \alpha_4^2[1 - 0.370x] + y\left[\frac{\mathcal{I}_0}{\mathcal{I}_>} - 1\right] \right\} . \quad \text{(A10)}$$

In Eq. (A10), $E^{(0)}_{\text{surf}}$ is the surface energy of the spherical nucleus[22]:

$$E^{(0)}_{\text{surf}} = 17.9439\eta A^{2/3} \text{ MeV} ; \quad \text{(A11)}$$

$\mathcal{I}_0$ is the rigid-sphere moment of inertia:

$$\mathcal{I}_0/\hbar^2 = 0.01448 A^{5/3} \text{ MeV}^{-1} ; \quad \text{(A12)}$$

and $\mathcal{I}_>$ represents the larger of the two moments of inertia $\mathcal{I}_{||}$ and $\mathcal{I}_\perp$, corresponding to rotations about the symmetry axis and about the orthogonal axes, respectively. For the rigid-body moments of inertia, integration over the deformed matter distribution [assumed to have a sharp surface at $R(\theta)$ from Eq. (A1)] yields:

$$\mathcal{I}_{||}/\mathcal{I}_0 = 1 - \alpha_2 + 0.429\alpha_2^2 + 0.268\alpha_2^3 - 0.212\alpha_2^4 - 1.143\alpha_2\alpha_4 + 0.494\alpha_2^2\alpha_4 + 0.266\alpha_4^2 ; \quad \text{(A13)}$$

$$\mathcal{I}_\perp/\mathcal{I}_0 = 1 + 0.5\alpha_2 + 1.286\alpha_2^2 + 0.581\alpha_2^3 - 0.451\alpha_2^4 + 0.571\alpha_2\alpha_4 + 1.897\alpha_2^2\alpha_4 + 0.700\alpha_4^2 . \quad \text{(A14)}$$

Equations (A13) and (A14) are identical through order α_2^2 to the corresponding expressions given in Refs. 7 and 45, but they differ in the higher-order terms.

We also obtain from Eq. (A10) an approximate expression for the RLDM yrast deformation, valid when this deformation remains mild and oblate, i.e., as long as the angular momentum is not too close to the critical value at which the fission barrier vanishes. Using Eqs. (A7) and (A8) to replace α_4, and then retaining terms in the energy formula through third order in α_2 and first order in y, minimization of E with respect to α_2 yields

$$\alpha_2^{\text{yrast}} \simeq -1.25y/(1-x) . \quad \text{(A15)}$$

Equation (A15) is used in MBEGAT in deciding whether the collective cutoff deformation [Eq. (44)] exceeds the RLDM yrast value in magnitude.

The electrostatic quadrupole interaction between an emitted charged particle and the deformed daughter nucleus is included in the angle-dependent effective radial potential [Eq. (13)] used to compute barrier transmission coefficients by the method outlined in Sec. II C. An expansion for the static quadrupole moment needed here is taken from Ref. 45:

$$Q_2 = ZR_Q^2(1.20\alpha_2 + 0.685\alpha_2^2 + 0.069\alpha_2^3 - 0.100\alpha_2^4 + 1.371\alpha_2\alpha_4 + 1.122\alpha_2^2\alpha_4 + 0.347\alpha_4^2) . \quad \text{(A16)}$$

In evaluating Q_2 in the code, we take $R_Q^2 = 1.50A^{2/3}$ fm^2.

*On leave from Institute for Nuclear Research, Swierk, Poland.

[1]For an extensive up-to-date review of applications of statistical model analyses, see R. G. Stokstad, in *Heavy Ion Science,* edited by D. A. Bromley (Plenum, New York, 1982) (to be published).

[2]S. E. Vigdor, Nukleonika (to be published), and references therein.

[3]A. Faessler, M. Ploszajczak, and K. W. Schmid, Prog. Part. Nucl. Phys. (to be published).

[4]M. Beckerman and M. Blann, Phys. Rev. Lett. 38, 272 (1977); Phys. Lett. 68B, 31 (1977); Phys. Rev. C 17, 1615 (1978).

[5]F. Plasil, *Proceedings of the International Conference on Reactions Between Complex Nuclei, Nashville, Tennessee, 1974,* edited by R. L. Robinson *et al.* (North-Holland, Amsterdam, 1974), Vol. 2, p. 107; F. Plasil, Phys. Rev. C 17, 823 (1978); F. Plasil, R. L. Ferguson, R. L. Hahn, F. E. Obenshain, F. Pleasonton, and G. R. Young, Phys. Rev. Lett. 45, 333 (1980).

[6]H. Delagrange, A. Fleury, and J. M. Alexander, Phys. Rev. C 16, 706 (1977).

[7]H. Hagelund and A. S. Jensen, Phys. Scr. 15, 225 (1977); J. U. Andersen, A. S. Jensen, K. Jørgensen, E. Laegsgaard, K. O. Nielsen, J. S. Forster, I. V. Mitchell, D. Ward, W. M. Gibson, and J. J. Cuomo, K. Dan. Vidensk. Selsk. Mat. Fys. Medd. 40, No. 7 (1980).

[8]T. Ericson, Adv. Phys. 9, 425 (1960).

[9]M. A. McMahan and J. M. Alexander, Phys. Rev. C 21, 1261 (1980).

[10]M. Blann, Phys. Rev. C 21, 1770 (1980).

[11]J. R. Huizenga and L. G. Moretto, Annu. Rev. Nucl. Sci. 22, 427 (1972).

[12]J. R. Huizenga, A. N. Behkami, J. S. Sventek, and R. W. Atcher, Nucl. Phys. A223, 577 (1974).

[13]J. R. Huizenga, A. N. Behkami, R. W. Atcher, J. S. Sventek, H. C. Britt, and H. Freiesleben, Nucl. Phys. A223, 589 (1974).

[14]T. Døssing and A. S. Jensen, Nucl. Phys. A222, 493 (1974).

[15]M. Beckerman, in *Theory and Applications of Moment Methods in Many-Fermion Systems,* edited by B. Dalton *et al.* (Plenum, New York, 1980).

[16]S. E. Vigdor, H. J. Karwowski, W. W. Jacobs, S. Kailas, P. P. Singh, F. Soga, and T. G. Throwe, Phys. Rev. C 26, 1035 (1982), the preceding paper.

[17]T. Ericson, Nucl. Phys. 6, 62 (1958).

[18]S. Bjørnholm, A. Bohr, and B. R. Mottelson, *Proceedings of the Third International Symposium on the Physics and Chemistry of Fission, Rochester, 1973* (International Atomic Energy Agency, Vienna, 1974), Vol. I, p. 367.

[19]D. W. Lang, Nucl. Phys. 77, 545 (1966).

[20]J. O. Rasmussen and K. Sugawara-Tanabe, Nucl. Phys. A171, 497 (1971).

[21]R. G. Stokstad and E. E. Gross, Phys. Rev. C 23, 281 (1981), and references therein.

[22]S. Cohen, F. Plasil, and W. J. Swiatecki, Ann. Phys. (N.Y.) 82, 557 (1974).

[23]C. J. Bishop, I. Halpern, R. W. Shaw, Jr., and R. Vandenbosch, Nucl. Phys. A198, 161 (1972).

[24]A. Bohr and B. R. Mottelson, *Nuclear Structure* (Benjamin, New York, 1969), Vol. I; *Nuclear Structure* (Benjamin, Reading, 1975), Vol. II.

[25]L. G. Moretto, Nucl. Phys. A182, 641 (1972).

[26]M. Beckerman and M. Blann, University of Rochester Internal Report UR-NSRL-135, 1977 (unpublished).

[27]N. Bohr and J. A. Wheeler, Phys. Rev. 56, 426 (1939).

[28]S. E. Vigdor, H. J. Karwowski, W. W. Jacobs, S. Kailas, P. P. Singh, F. Soga, and P. Yip, Phys. Lett. 90B, 384 (1980).

[29]I. Halpern and V. M. Strutinski, *Proceedings of the Second U.N. International Conference on Peaceful Uses of Atomic Energy* (United Nations, New York, 1959), Vol. 15, p. 408.

[30]R. Vandenbosch and J. R. Huizenga, *Nuclear Fission* (Academic, New York, 1973).

[31]C. Y. Fu and F. G. Perey, At. Data Nucl. Data Tables 16, 409 (1975); T. Mo and R. H. Davis, Phys. Rev. C 6, 231 (1972); W. T. H. van Oers, H. Haw, N. E. Davison, A. Ingemarsson, B. Fagerstrom, and G. Tibell, *ibid.* 10, 307 (1974); G. M. Hudson and R. H. Davis, *ibid.* 10, 1521 (1974).

[32]P. O. Fröman, K. Dan. Vidensk. Selsk. Mat. Fys. Medd. 1, No. 3 (1957).

[33]D. L. Hill and J. A. Wheeler, Phys. Rev. 89, 1102 (1953).

[34]J. M. Alexander, L. C. Vaz, and S. Y. Lin, Phys. Rev. Lett. 33, 1487 (1974).

[35]We distinguish here between the *state* density Ω and the *level* density ρ. The former includes, and the latter does not, the $(2I+1)$ magnetic substates associated with each level of total angular momentum I.

[36]A. Gavron, Phys. Rev. C 21, 230 (1980).

[37]S. K. Kataria, V. S. Ramamurthy, and S. S. Kapoor, Phys. Rev. C 18, 549 (1978); V. S. Ramamurthy, S. K. Kataria, and S. S. Kapoor, Nucl. Phys. A334, 477 (1980).

[38]L. G. Moretto, *Proceedings of the Third International Symposium on the Physics and Chemistry of Fission, Rochester, 1973* (International Atomic Energy Agency, Vienna, 1974), Vol. I, p. 329.

[39]A. V. Ignatyuk, G. N. Smirenkin, and A. S. Tishin, Yad. Fiz. 21, 485 (1975) [Sov. J. Nucl. Phys. 21, 255 (1975)].

[40]D. W. Lang and K. J. LeCouteur, Nucl. Phys. 14, 21 (1959).

[41]A. V. Ignatyuk, K. K. Istekov, and G. N. Smirenkin, Yad. Fiz. 29, 875 (1979) [Sov. J. Nucl. Phys. 30, 626 (1979)].

[42]R. Bass, Nucl. Phys. A231, 45 (1974).

[43]U. Mosel, P. G. Zint, and K. H. Passler, Nucl. Phys. A236, 252 (1974).

[44]W. J. Swiatecki, Phys. Rev. 104, 993 (1956).

[45]M. Brack, T. Ledergerber, H. C. Pauli, and A. S. Jensen, Nucl. Phys. A234, 185 (1974).